

# Antibacterial Performance of Fe<sub>2</sub>O<sub>3</sub> Nanoparticles Synthesized via Biosynthesis from Chitosan

<sup>1</sup>Faisal J. Kadhim\*, <sup>2</sup>Mohamed Hedi Bedoui, <sup>3</sup>Ali A. Turki Aldalawi

<sup>1</sup>Physics of Department, Faculty of Science of Monastir (FSM), University of Monastir, Tunisia

<sup>2</sup>Medical Technology and Imaging Laboratory, Faculty of Medicine of Monastir, University of Monastir, Tunisia

<sup>3</sup>School of Physics, University of Science Malaysia (USM), Malaysia

## ARTICLE INFO

### Article history:

Received: November, 06, 2024

Accepted: May, 09, 2025

Available online: June, 10, 2025

### Keywords:

Fe<sub>2</sub>O<sub>3</sub> NPs,

Chitosan,

Antibacterial activity,

Hydrothermal method,

Bio-composite

### \*Corresponding Author:

Faisal J. Kadhim

[Faisaljabbar35@gmail.com](mailto:Faisaljabbar35@gmail.com)

## ABSTRACT

In this study, Fe<sub>2</sub>O<sub>3</sub> nanoparticles were synthesized by a hydrothermal method using chitosan extract and ferric chloride (FeCl<sub>3</sub>) as precursor at 150 °C. The hydrothermal approach provides precise control over the size and morphology of the nanoparticles by promoting the decomposition and crystallization of the precursors near their evaporation temperatures. The aim of this study was to quantify the antibacterial activity of the nanoparticles to regulate the production of Fe<sub>2</sub>O<sub>3</sub> NPs. The optical and structural properties of Fe<sub>2</sub>O<sub>3</sub> nanoparticles (NPs) were investigated and tested using various techniques, including X-ray diffraction (XRD), field emission scanning electron microscopy (FESEM), ultraviolet-visible (UV-vis) spectroscopy and photoluminescence (PL). The crystal size and hexagonal structure of Fe<sub>2</sub>O<sub>3</sub> NPs in the range of 10 to 25 nm were determined by XRD. In addition, FESEM images were used for measurement. The morphology and particle size of the Fe<sub>2</sub>O<sub>3</sub> NPs, which is between 15.63 and 56.84 nm due to the aggregation of the nanoparticles. The UV-visible spectra were used to calculate the direct and indirect optical band gap versus  $h\nu$  of the Fe<sub>2</sub>O<sub>3</sub> NPs prepared by the hydrothermal method from chitosan extract NPs. These are 3.8 eV and 3.6 eV, respectively. The band edge emission of Fe<sub>2</sub>O<sub>3</sub> NPs was about 2.57 eV as measured by photoluminescence (PL) spectroscopy. Inhibition zones of 40 mm in size were observed for *Staphylococcus aureus* and *Escherichia coli*.

<https://doi.org/10.53293/jasn.2025.7540.1329>, Department of Applied Sciences, University of Technology - Iraq.

© 2025 The Author(s). This is an open access article under the CC BY license (<http://creativecommons.org/licenses/by/4.0/>).

## 1. Introduction

In recent times, nanomaterials have emerged as a very captivating and cutting-edge topic within the realms of science and technology. Nanoparticles (NPs) have gained significant attention due to the growing need for environmentally benign approaches to material processing. The domains of technological innovation have gained significance [1]. Several synthesis techniques have discovered diverse uses for nanoparticles of different sorts, each with distinct characteristics [2]. Iron oxide nanoparticles have garnered significant interest due to their distinctive magnetic, optical, and electrical properties [3]. Magnetic nanoparticles have been synthesized using

many techniques, such as hydrothermal process, microemulsion, thermal breakdown, sol-gel processing, co-precipitation, and other approaches [4].

Additionally, the efficacy of transition metal oxides, including NiO, MnO<sub>2</sub>, Fe<sub>2</sub>O<sub>4</sub> NPs nanoparticles, and Fe<sub>2</sub>O<sub>3</sub> nanoparticles, was examined as super capacitor electrode materials [5]. Iron oxide (Fe<sub>2</sub>O<sub>3</sub>) is a stable, advantageous compound ecologically benign and facile to synthesize. It possesses a band gap of 2.1 eV, making it an outstanding candidate for the absorption of visible solar light. Many researchers have focused on enhancing the optical, electrical, and mechanical properties of polymers by integrating fillers for various applications [6]. Utilized a chemical method to synthesize iron oxide nanoparticles (IONPs) using Lawsonia inermis (henna) extract [7]. In 2019, produced Fe<sub>2</sub>O<sub>3</sub> NPs served as a catalyst for the degradation of methylene blue (MB) utilizing extracts from Galinsoga parviflora, Conyza bonariensis, and Bidens pilosa, in addition to employing a chemical approach. Pulsed laser ablation, particularly using Nd-YAG lasers, is a prevalent method for synthesizing nanoparticles in liquid environments. This method effectively fabricates nanomaterial's by swiftly reacting and cooling ablated particles at the plasma-liquid interface [8].

Compared to physical and chemical processes, green synthesis has the advantage of being both economical and environmentally friendly. It requires no hazardous chemicals, works at low temperatures and consumes very little energy. It can also be produced on a large scale. Green synthesis improves the regulation of crystal development. Ecologically synthesized nanoparticles are inexpensive and offer numerous scientific applications [9-11]. Iron oxide has several advantages, including a small band gap energy of about 2.2 eV, affordability, lack of toxicity, wide availability, and thermal stability. Magnetite consists of two forms of iron, ferrous and ferric. Therefore, it is commonly referred to as ferric and ferrous oxide. There are three main forms of iron oxides that occur in nature: Maghemite ( $\gamma$ - Fe<sub>2</sub>O<sub>3</sub>), magnetite (Fe<sub>2</sub>O<sub>4</sub>) and hematite ( $\alpha$ - Fe<sub>2</sub>O<sub>3</sub>) [12]. The ability of Fe<sub>2</sub>O<sub>3</sub> NPs to hinder vital enzyme processes in microbes is another inhibitory mechanism. They interfere with metabolic processes and slowing or stopping cell growth, for example by blocking enzymes required for cellular respiration and energy production [13], as shown in **Fig. 1** [14].

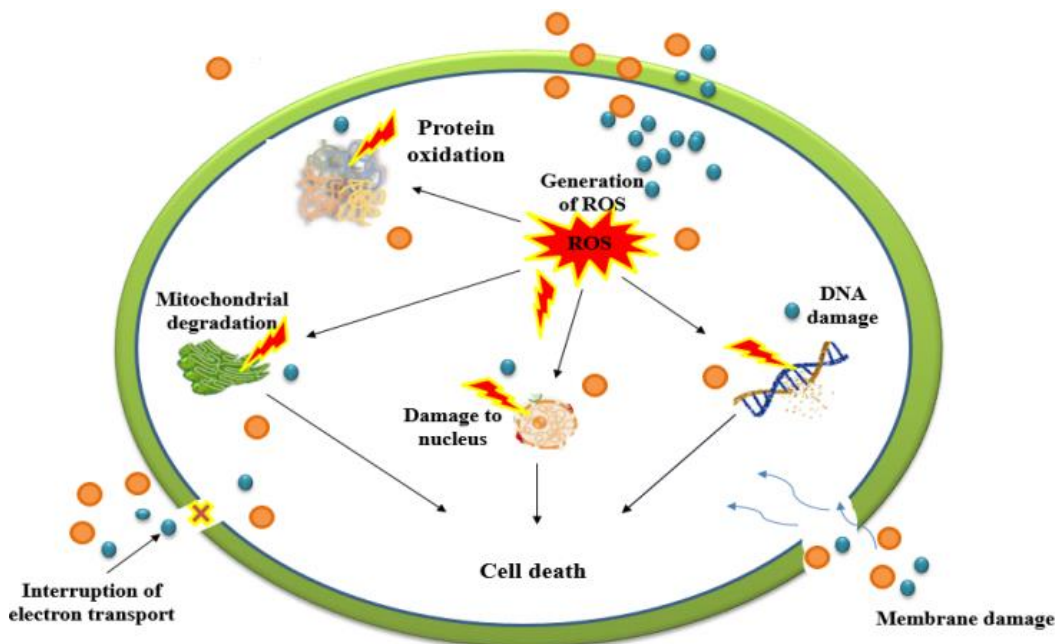


**Figure 1:** Proposed mechanism of Fe<sub>2</sub>O<sub>3</sub> NP antibacterial action [13].

In this study, a hydrothermal method was used to synthesize Fe<sub>2</sub>O<sub>3</sub> nanoparticles (NPs) at 400 °C by mixing chitosan with ferric chloride (FeCl<sub>3</sub>). Many techniques have been used to examine and characterize the optical and structural properties of the Fe<sub>2</sub>O<sub>3</sub> NPs, for example, X-ray diffraction (XRD), field-emission scanning electron microscopy (FESEM), UV-visible spectroscopy (UV-vis), and photoluminescence (PL) spectra.

The novelty of this study involves the synthesis of a composite material by combining ferric chloride ( $\text{FeCl}_3$ ) salt with chitosan extract. This composite significantly enhances the bactericidal activity of  $\text{Fe}_2\text{O}_3$  NPs, demonstrating the effective elimination of harmful bacteria and microbes. Our results successfully showcase the improved antibacterial capabilities of this composite material. Furthermore, the hydrothermal approach demonstrated exceptional efficacy in generating nanoparticles of great quality. The resultant  $\text{Fe}_2\text{O}_3$  nanoparticles are safe, non-toxic, economical, and environmentally benign, with a well-defined crystalline structure. This research highlights the efficacy of the hydrothermal technique and chitosan-based synthesis in the creation of high-performance antibacterial materials.

## 2. Experimental work:

### 2.1. Materials and Methods

The ferric chloride ( $\text{FeCl}_3$ ) salt, with a purity of 99.99%, and chitosan extract powder were purchased from the local supplier in Iraq. The chitosan extract contains a substantial number of organic polysaccharides, proteins, and cellulose. The investigation made use of Borosil glassware. Distilled water, a magnetic stirrer, and locally sourced chitosan extract solutions were combined.

### 2.2. Create of Chitosan Extract

We used 5 grams of chitosan powder and 100 mL of distilled water to produce the final solution of extract after that the mixture was placed on a magnetic stirrer until it reached a temperature of 60 °C for a minimum of two hours. In order to achieve the best possible results, we filtered the combination by means of the Whatman filter sheet and then brought it down to room temperature [15]. We stored the extract powder at less than 37 °C for future use. Please refer to **Fig. 2** for a detailed explanation of all the processes involved in transforming the newly obtained mixture into the final chitosan extract samples.

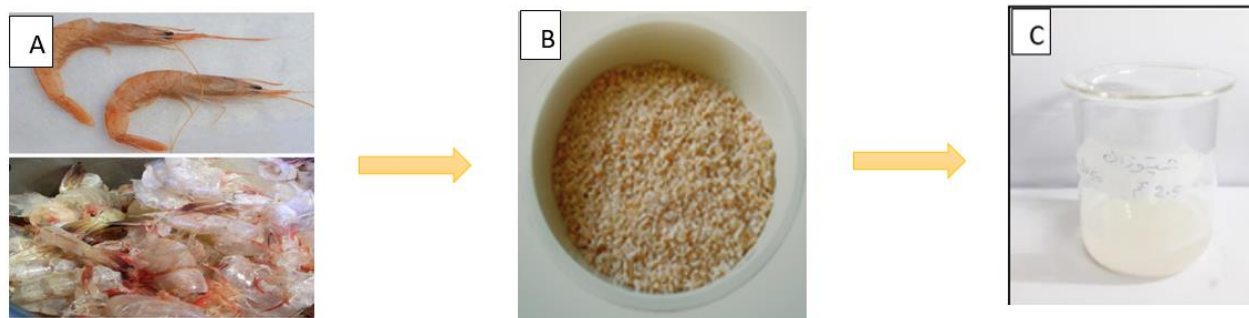


**Figure 2:** Extraction process of chitin from shrimp shell waste (A) Cambrian, (B) chitosan powder, (C) chitosan extract.

### 2.3. Synthesis of $\text{Fe}_2\text{O}_3$ NPs

Iron oxide (III) occurs naturally as rust. Iron oxides are ubiquitous, commonly employed for their affordability, and are integral to various geological and biological processes. A recent study indicates that natural hematite can serve as a cathode material and is utilized in developing microbial fuel cells. Maghemite, magnetite, or any ferrite with a size under 100 nm and super paramagnetic properties constitute SPIONs [16]. In our work, we used hydrothermal synthesis for nanoparticle production, utilizing an extensive temperature spectrum from ambient to extremely high temperatures. Contrasting this strategy with physical and biological approaches presents numerous advantages.

Producing  $\text{Fe}_2\text{O}_3$  nanoparticles involves combining 50 mL of extract powder with 50 mL of a 0.5 M solution of  $\text{FeCl}_3$ , resulting in a freshly formed solution. The follow-up phase increased. The mixture was prepared using a hotplate stirrer at a temperature of 70 °C for 45 minutes. The producing of  $\text{Fe}_2\text{O}_3$  NPs was noticed by altering the reaction solution color from white to black. We permitted the solution to equilibrate with the ambient temperature. A volume of 15 mL of the  $\text{Fe}_2\text{O}_3$  NPs solution was placed in a ceramic container, subsequently heated to 400 °C for three hours. After that, we proceeded to deposit the powdered  $\text{Fe}_2\text{O}_3$  nanoparticles into serum vials that were properly sealed so that we could do further analysis [16] as shown in the **Fig. 3**.

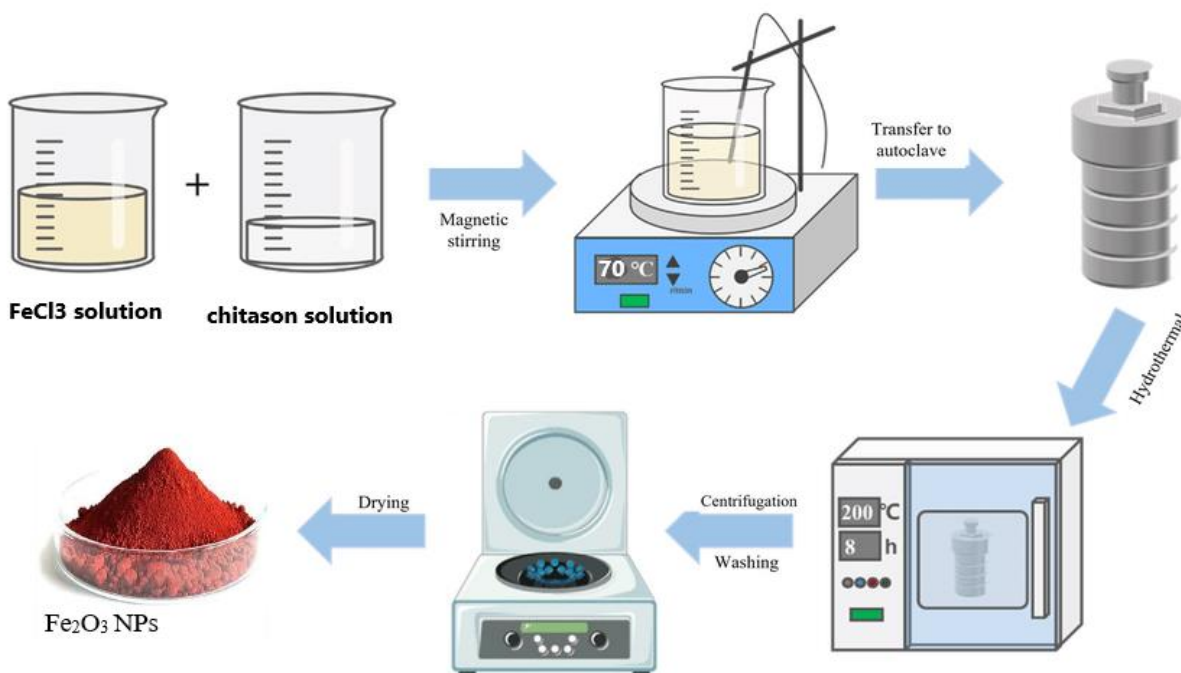


**Figure 3:** Stages to convert the mixture into Fe<sub>2</sub>O<sub>3</sub> NPs via hydrothermal method.

#### 2.4. Antibacterial Activity of Fe<sub>2</sub>O<sub>3</sub> NPs

Antibiotics are artificial or natural substances that can destroy or inhibit bacterial growth without inducing harm in surrounding tissues. Nanotechnology offers the potential to reevaluate the biological properties of previously recognized antibacterial agents by modifying their dimensions to alter their effects. Fe<sub>2</sub>O<sub>3</sub> NPs exhibited high efficacy in bacterial culture plates, eliciting dose-dependent alterations in inhibitory zone measurements. More inhibition of the gram-negative *Escherichia coli* (*E. coli*) zone was noted in the Fe<sub>2</sub>O<sub>3</sub> NPs created from FeCl<sub>3</sub> salt and chitosan extract at a temperature of 400 °C. This was in contrast to the gram-positive bacterium *Staphylococcus aureus* (*S. aureus*). This variety may stem from the intrinsic variability in the formation of the cell wall of gram-negative bacteria. Gram-positive bacteria form a strong peptidoglycan layer of proteins, lipopolysaccharides, and phospholipids [17]. The biosynthesized Fe<sub>2</sub>O<sub>3</sub> NPs exhibited antibacterial activity against all examined bacterial species. The bactericidal efficacy of Fe<sub>2</sub>O<sub>3</sub> NPs nanoparticles were observed to be greater against Gram-negative bacteria than Gram-positive bacteria, according to the differences in their structural makeup.

Here, the bactericidal effect of the previously made Fe<sub>2</sub>O<sub>3</sub> NPs will be visible. The cell membrane permeability to the metal ion-produced reactive oxygen species (ROS), the cell's thickness, and the cell wrapper's shape are all prerequisites for this effect to materialize. Nanoparticles fabricated from Iron oxide have shown antimicrobial properties through various mechanisms. These qualities encompass the capacity to traverse cell membranes, the breakdown of oxygen species interacting, and the liberation of DNA and volatile metals that impede the aerobic cycle and cell division [18]. Incorporation can lead to several results, such as cell lysis, exocytosis, DNA injection, or the deactivation of vital enzymes causing cellular harm. We calculated the proportion of the obstructed zone using the provided **Eq. (1)** [19]:

$$\text{Inhibition Zone \%} = \frac{\text{Diameter of the inhibition zone (mm)}}{\text{petriplate Diameter (90 mm)}} \times 100\% \quad (1)$$

### 3. Results and Discussion

#### 3.1. XRD Analysis

Fig. 4 exhibits the strong peaks (101) and (204), which signify the preferred orientation of Fe<sub>2</sub>O<sub>3</sub> NPs at a temperature of 400 °C. Furthermore, there are other important peaks, including (100), (101), (204), (207), and (300). This outcome aligns with [20-22]. Table 1, XRD analysis displays the characteristics of iron (III) oxide nanoparticles (Fe<sub>2</sub>O<sub>3</sub> NPs) at a temperature of 400 °C using an extract obtained from chitosan. From Scherer's equation Eq. (2), we can calculate the crystallite size [7, 23].

$$D = k \lambda / \beta \cos\theta \tag{2}$$

Where (D): is the size of crystallite, ( $\lambda$ ): X-ray wavelength (1.5406 Å), ( $\beta$ ): represent of (FWHM) of the peaks, (K): Scherer's constant (0.9), ( $\theta$ ): the diffraction angle

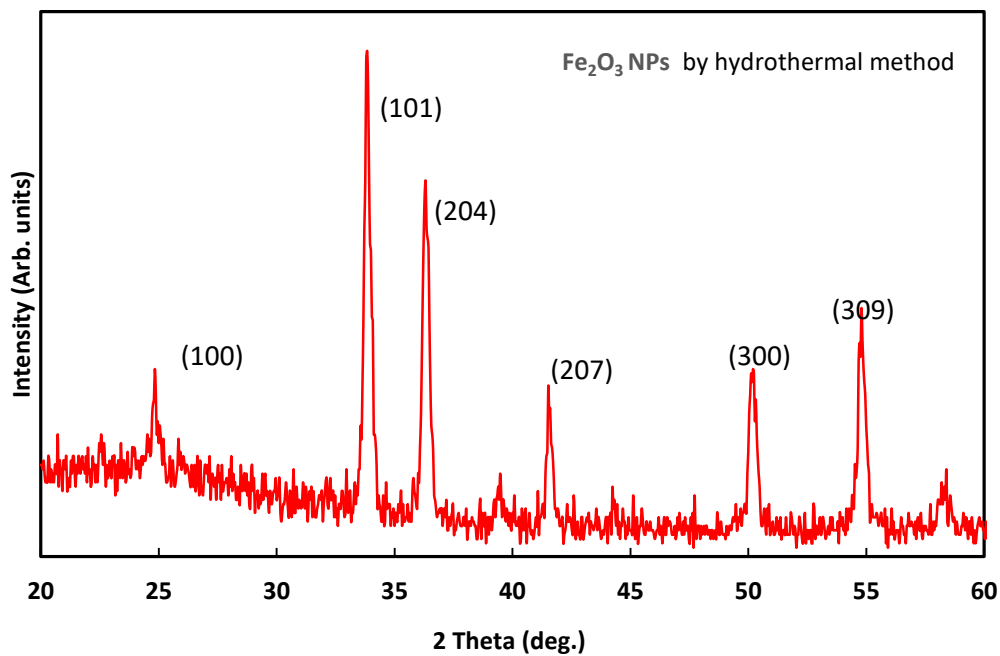


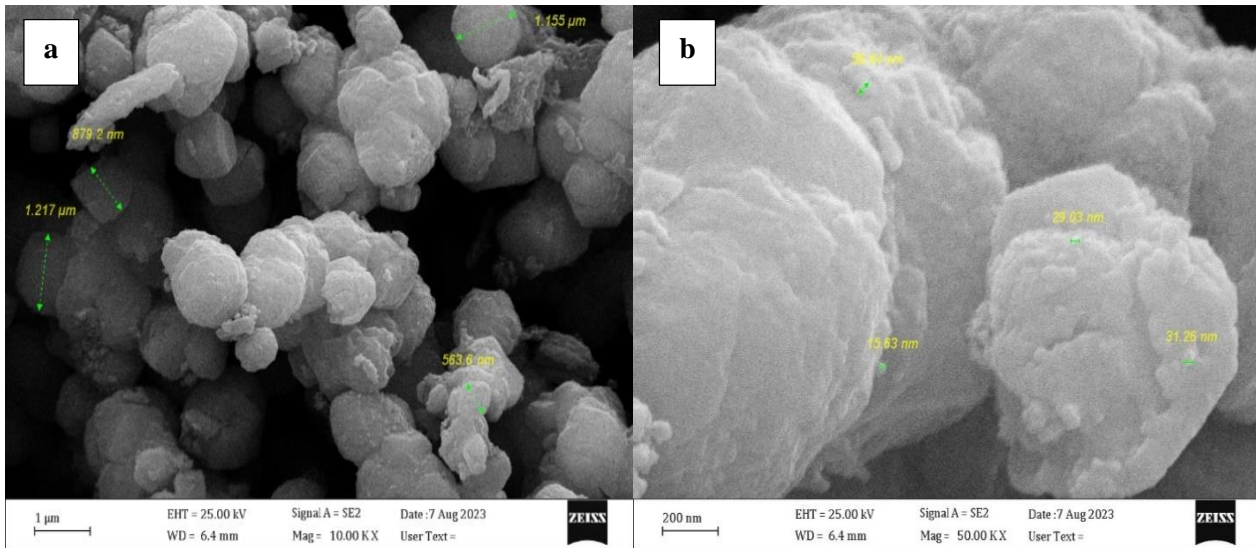
Figure 4: XRD patterns of Fe<sub>2</sub>O<sub>3</sub> NPs obtained from the chitosan extract using the hydrothermal technique.

Table 1: The calculations were performed on Fe<sub>2</sub>O<sub>3</sub> NPs that were produced using a chitosan.

| Material         | Phase                              | 2θ(deg.) | β(deg.) | θ(rad) | β(rad) | D(nm)    |
|------------------|------------------------------------|----------|---------|--------|--------|----------|
| Chitosan extract | Fe <sub>2</sub> O <sub>3</sub> NPs | 25.9     | 0.48    | 0.235  | 0.010  | 16.89285 |
|                  |                                    | 34.8     | 0.56    | 0.270  | 0.009  | 14.79133 |
|                  |                                    | 36.4     | 0.80    | 0.319  | 0.015  | 10.40096 |
|                  |                                    | 41.7     | 0.61    | 0.348  | 0.012  | 13.86868 |
|                  |                                    | 50.2     | 0.52    | 0.475  | 0.010  | 16.79489 |
|                  |                                    | 55.6     | 0.86    | 0.514  | 0.013  | 15.0605  |

### 3.2. FESEM Analysis of Fe<sub>2</sub>O<sub>3</sub> NPs Derived Chitosan Extract

**Fig. 5** illustrates the FESEM analysis of Fe<sub>2</sub>O<sub>3</sub> nanoparticles produced on a glass substrate utilizing chitosan extract as a green synthesis technique. We then analyzed the shape and mean grain size of Fe<sub>2</sub>O<sub>3</sub> nanoparticle nanoparticles. The micrograph displayed in the image showcases pleasing nanoparticle structures with grain sizes ranging from 15.63 to 56.84 nm. The particles display a mostly semispherical morphology. The chitosan extract synthesis process it is distinguished by its eco-friendly and environmentally method reducing the reliance on toxic chemicals. The FESEM study confirms the effective fabrication of Fe<sub>2</sub>O<sub>3</sub> nanoparticle nanoparticles and presents deep insights into their morphological characteristics. The observed semispherical shape signifies the uniform nucleation and growth process promoted by the chitosan extract, which serves as a stabilizing and capping agent. The investigation of the size distribution of the nanoparticles reveals a reasonably limited range, which is beneficial for applications necessitating uniformity in particle size, including catalysis, sensors, and biological sectors. The found nanostructures are anticipated to demonstrate increased surface area and reactivity, essential for their efficacy in diverse applications. The FESEM micrograph in **Fig. 5** highlights the effectiveness of chitosan extract in the green synthesis of Fe<sub>2</sub>O<sub>3</sub> nanoparticles, exhibiting distinct shapes and homogeneous grain size distribution. This synthesis method possesses considerable potential for the scalable creation of nanomaterials with advantageous characteristics for various technological applications.



**Figure 5:** FESEM images of Fe<sub>2</sub>O<sub>3</sub> nanoparticles at (a) low magnification and (b) high magnification.

### 3.3. UV-Visible

Analytical methods such as UV-Vis spectroscopy measure how much light a sample absorbs or transmits at certain ultraviolet (UV) and visible (visible) wavelengths in comparison to a control (or blank) sample. This characteristic, which might reveal the sample's components and concentrations, is affected by the sample's composition. Furthermore, ultraviolet-visible spectroscopy is considered a major examination for studying UV-visible spectroscopy; we can measure the transmittance of Fe<sub>2</sub>O<sub>3</sub> NPs and then use that information to figure it out. As shown in **Fig. 6a**, according to their corresponding wavelength of 300 nm and the proportion of absorbance of the Fe<sub>2</sub>O<sub>3</sub> NPs, we calculated the direct and indirect optical band gap versus  $h\nu$  of Fe<sub>2</sub>O<sub>3</sub> NPs created from chitosan extract NPs via hydrothermal method are 3.8 eV and 3.6 eV respectively, as shown in **Fig. 6b and c**. The Tauc plot **Eq. (3)** used to calculate the energy band gap ( $E_g$ )

$$(ah\nu)^2 = \beta(h\nu - E_g) \quad (3)$$

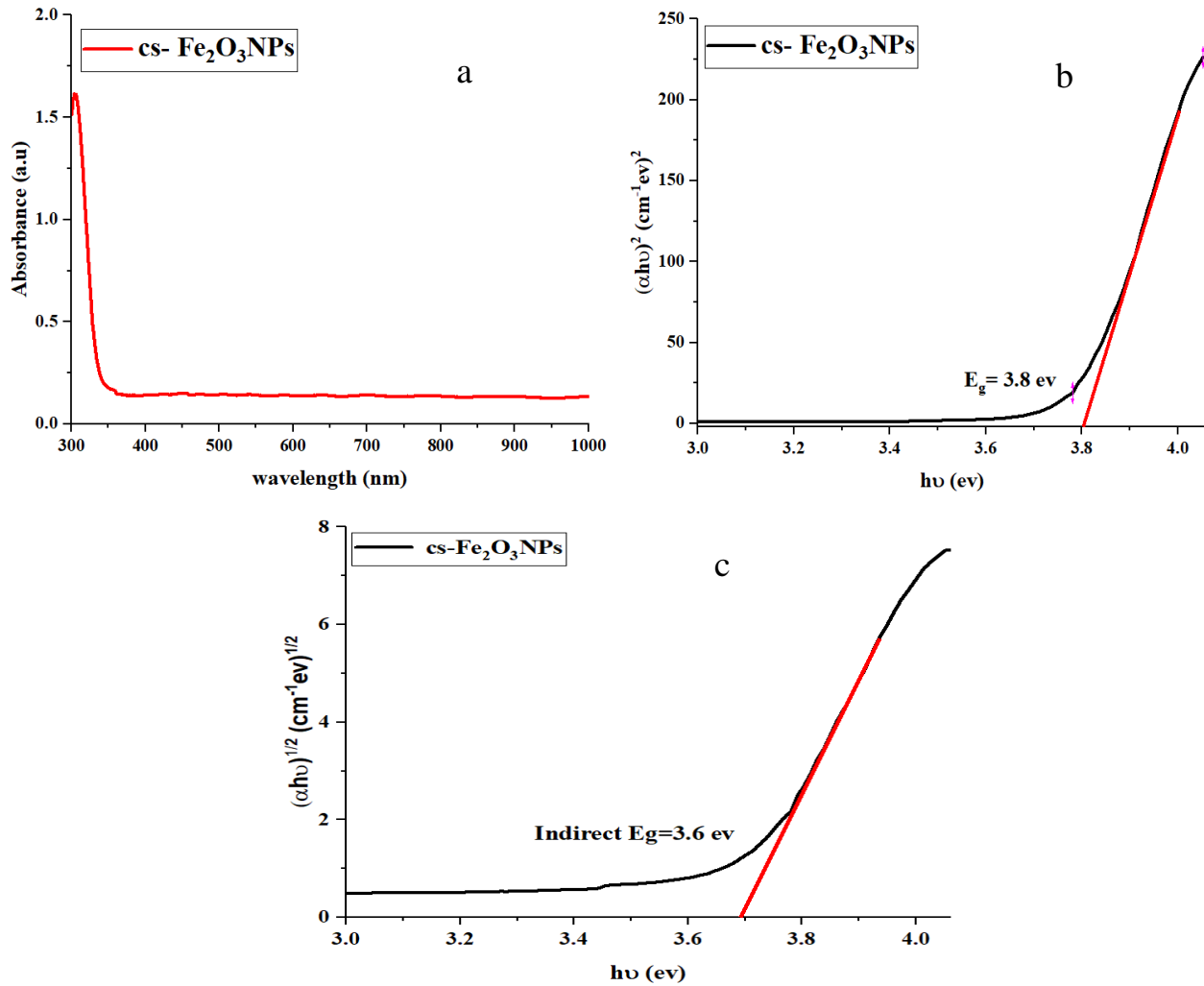


**Figure 6:** UV–Vis absorbance spectrum (a), Tauc plot for direct band gap (b), and Tauc plot for indirect band gap (c) of Fe<sub>2</sub>O<sub>3</sub> nanoparticles.

### 3.4. Photoluminescence Spectrum of IONPs

When a molecule absorbs a visible-light photon, it excites one of its electrons to a more excited electronic state; when the electron returns to a lower energy level, it radiates another photon, a process known as photoluminescence [24]. The data given exhibits the photoluminescence spectra of the Fe<sub>2</sub>O<sub>3</sub> NPs produced by mixing the chitosan extract and FeCl<sub>3</sub> salt using the hydrothermal technique. **Fig. 7** shows the following stimulation of the Fe<sub>2</sub>O<sub>3</sub> NPs at room temperature using a 325 nm He-Cd laser. The sample of Fe<sub>2</sub>O<sub>3</sub> NPs was illuminated by a single broad-spectrum, weak-edge emission from this laser, with a center wavelength of around 315 nm. The value of the near band edge was determined to be 2.57 eV, in agreement with previous research findings [25].

On the other hand, the **Eq. (4)** was used to calculate the near–band edges:

$$E_g = hc/\lambda_{NBE} \tag{4}$$

Where  $\lambda_{NBE}$  is a near-band edge (NBE) luminescence.

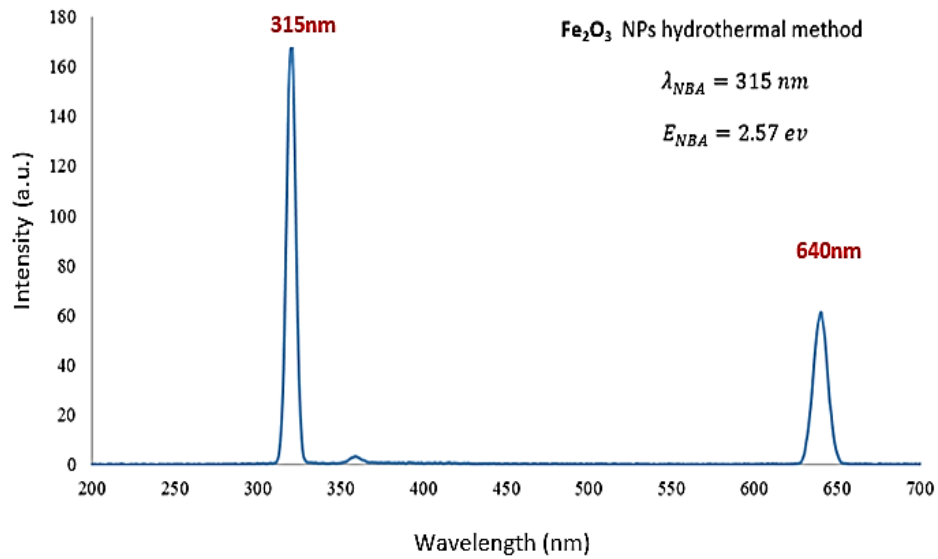


**Figure 7:** Photoluminescence spectrum of Fe<sub>2</sub>O<sub>3</sub> NPs prepared via hydrothermal technique.

This leads to a strong correlation with the findings derived from UV/Vis measurements, where the indirect band gap determined by UV/Vis spectroscopy is 4.2 eV. This study illustrates the Hydrothermal technique's efficacy in significantly altering a material's energy band gap. Furthermore, imperfections inside the material might substantially impact the photoluminescence behavior. Unoccupied positions within the crystal structure can form certain energy levels in a confined manner. These energy levels affect the electronic transitions that are responsible for the emission of PL wavelengths. Furthermore, the presence of impurities, such as accidental dopants, has the potential to alter the state of the electrical configuration, which in turn affects the emission spectrum. These findings align with the UV-vis data stated before [26].

Furthermore, the below **Table 2**, summaries various Applications and methods employed for the synthesis of magnetic iron oxide.

**Table 2:** Comparative analysis of various methods employed for the synthesis of magnetic iron oxide.

| Method                    | Plant extract | Material                         | Plane (hkl)                      | Crystallite size D (nm) | Applications   | Ref. |
|---------------------------|---------------|----------------------------------|----------------------------------|-------------------------|--|------|
| This work<br>Hydrothermal | Chitosan      | Fe <sub>2</sub> O <sub>3</sub>   | 100                              | 16.89285                | Antibacterial activity against <i>S. aureus</i> and <i>E. coli</i> Bacteria. |      |
|                           |               |                                  | 204                              |                         |  |      |
| Simple chemical           | Conocarpus    | β-Fe <sub>2</sub> O <sub>3</sub> | 201                              | 14.79133                | Antibacterial activity against <i>S. aureus</i> and <i>E. coli</i> Bacteria. | [27] |
|                           |               |                                  | 207                              | 10.40096                |  |      |
|                           |               |                                  | 0217                             | 13.86868                | Semiconductor devices  |      |
| Sol-gel                   | Conocarpus    | β-Fe <sub>2</sub> O <sub>3</sub> | 006                              | 3.310491                | Photonics, catalysis and biosensors.   | [27] |
|                           |               |                                  | 102                              | 39.65497                | Antibacterial activity   |      |
|                           |               |                                  | γ-Fe <sub>2</sub> O <sub>3</sub> | 4.6                     |  |      |
| Hydrothermal approach     |               | α-Fe <sub>2</sub> O <sub>3</sub> |                                  | ~400                    |  | [29] |
|                           |               |                                  |                                  | ~230                    |  |      |
|                           |               |                                  |                                  | 19                      |  |      |
|                           |               |                                  |                                  | 46                      |  |      |

|  |                  |                                      |          |                      |  |      |
|--|------------------|--------------------------------------|----------|----------------------|--|------|
|  |                  | Fe <sub>3</sub> O <sub>4</sub>       |          | 11.5<br>47.7<br>~150 | Antibacterial activity<br>against <i>S. aureus</i> and<br><i>E. coli</i> Bacteria. | [30] |
| PLA  |                  | Fe <sub>3</sub> O <sub>4</sub> /CNTs |          | 60 to 135<br>50      | Antibacterial  | [31] |
| Chemical method<br>with and without<br>(PLA) | Henna<br>extract | Iron oxide<br>NPs                    | 017      | 54                   | Photocatalytic activity  | [7]  |
|  |                  |                                      | 110      | 24                   |  |      |
|  |                  | Fe <sub>2</sub> O <sub>3</sub>       | 45<br>34 |                      |  |      |

### 3.5. Antibacterial Activity Test

Two harmful gram-positive bacteria *Mycobacterium aureus* and gram-negative bacteria an agar-based nutrient broth was prepared, and the antibacterial efficacy of Fe<sub>2</sub>O<sub>3</sub> nanoparticles was assessed against *E. coli* utilizing the Mueller-Hinton agar well diffusion method. Bacteria *S. aureus* or *E. coli* were uniformly dispersed around the surface of the Petri plate. Wells with a diameter of 6 mm were excised from each agar plate with a sterilized well cutter, as seen in **Fig. 8**. The antimicrobial properties of Fe<sub>2</sub>O<sub>3</sub> NPs produced through hydrothermal methods were investigated.

A diagrammatic representation of the inhibition zone for positive *S. aureus* and negative *E. coli* bacteria can be found in **Fig. 9**. In each of the three wells, which were numbered (4), (5), and (6), there was a concentration of approximately 30 mg/L of Fe<sub>2</sub>NO<sub>3</sub> salt (3), 30 mg/L of chitosan (4), and Fe<sub>2</sub>O<sub>3</sub> NPs obtained from chitosan extract (6), respectively. Following treatment of Fe<sub>2</sub>O<sub>3</sub> NPs with chitosan extract, it was discovered that the percentage of bacteria had been eliminated or eliminated. This is demonstrated in **Fig. 9**, which demonstrates that these results were exceptional compared to the other samples. The proteins in the chitosan extract had a more significant impact than the biomolecules themselves, which explains why this is the case. This finding is very encouraging and stands out compared to the results that were compared to those obtained previously. An explanation of the inhibition zone proportion (%) of Fe<sub>2</sub>O<sub>3</sub> NPs is provided in **Table 3**. The chitosan extract was created chemically and was at a concentration of 30 mg/L [33].

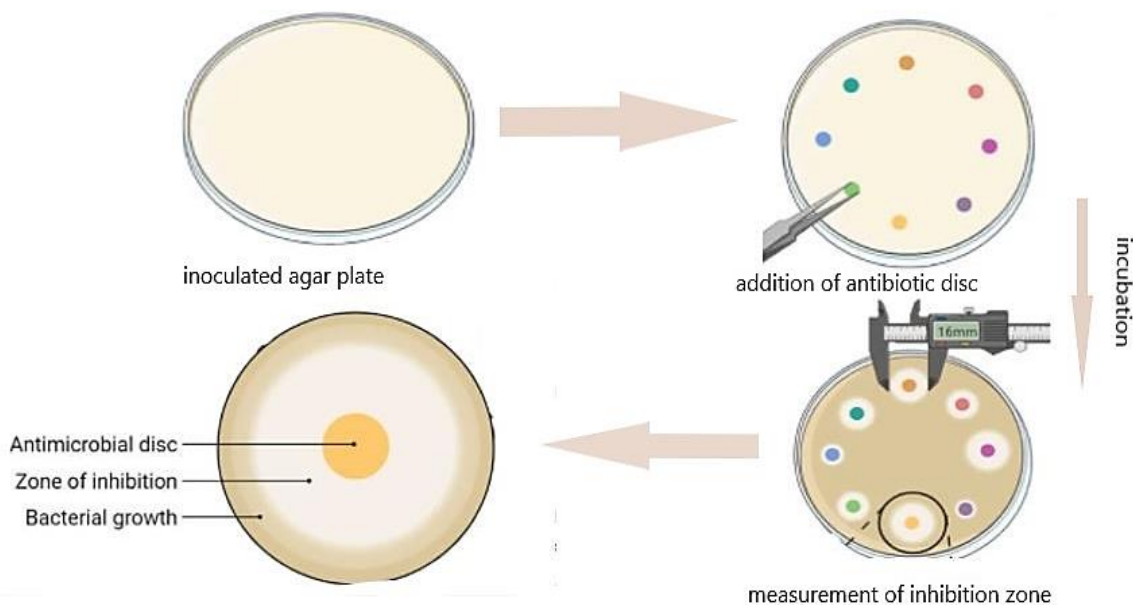


**Figure 8:** The Well diffusion assay for the antibacterial test.

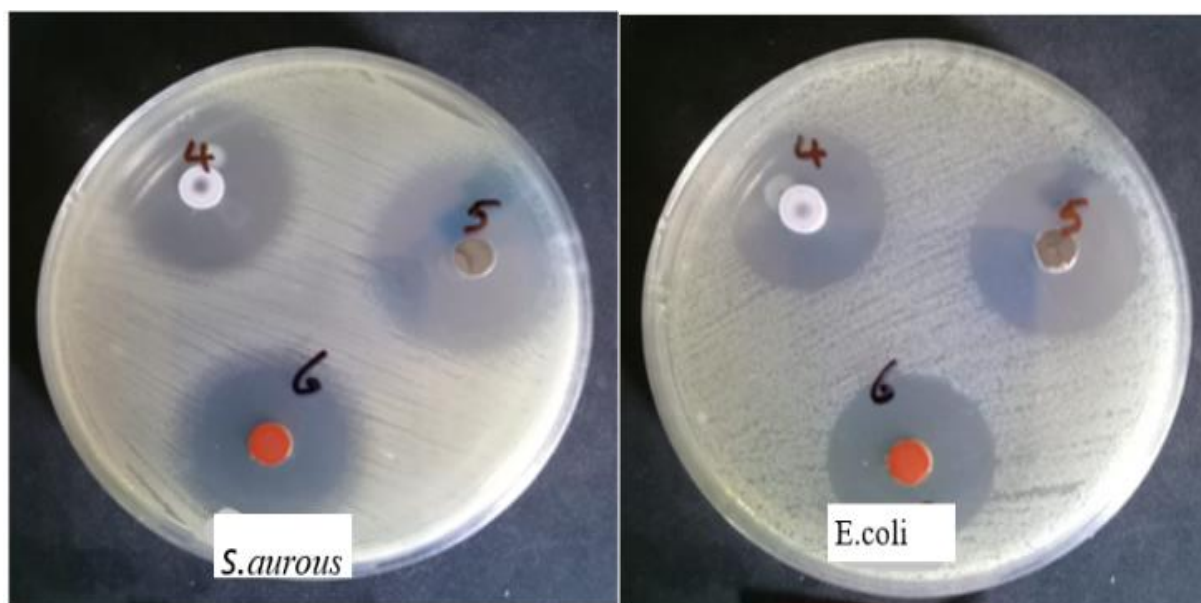


**Figure 9:** Antimicrobial effects of the  $\text{Fe}_2\text{O}_3$  NPs against (*S. aureus*) and (*E. coli*) and (30 mg/L). (4) ( $\text{FeCl}_3$ ) salt, (5) chitosan extract, and (6)  $\text{Fe}_2\text{O}_3$  NPs with chitosan extract.

**Table 3:** the inhibition zones of  $\text{Fe}_2\text{O}_3$  NPs prepared from chitosan extract.

| Extract  | Material                | Gram (-)            |                       | Gram (+)            |                       | Inhibition zone (%) |                       |
|----------|-------------------------|---------------------|-----------------------|---------------------|-----------------------|---------------------|-----------------------|
|          |                         | <i>E. coli</i> (mm) | <i>S. aureus</i> (mm) | <i>E. coli</i> (mm) | <i>S. aureus</i> (mm) | <i>E. coli</i> (mm) | <i>S. aureus</i> (mm) |
| Chitosan | $\text{Fe}_2\text{O}_3$ | 15                  | 15                    | 45.5                | 20                    |                     |                       |
|          |                         | 20                  | 20                    | 49.5                | 25                    |                     |                       |
|          |                         | 21                  | 21                    | 55                  | 26.3                  |                     |                       |

#### 4. Conclusions

The hydrothermal method successfully produced  $\text{Fe}_2\text{O}_3$  NPs from chitosan by combining ferric chloride ( $\text{FeCl}_3$ ) salt. The XRD study showed that the diffraction peaks have a satisfactory crystal quality for  $\text{Fe}_2\text{O}_3$  NPs and they can be particularly characterized as a hexagonal structure of  $\text{Fe}_2\text{O}_3$  NPs with a crystal size of 10 to 25 nm. The FESEM result also showed the presence of the  $\text{Fe}_2\text{O}_3$  NPs, which are very active because they have many surface-bound bonds and can easily react with solvents or aggregates. These particles are about 15.63 to 56.84 nm in size. According to PL spectroscopy, the band edge emission of  $\text{Fe}_2\text{O}_3$  NPs was about 2.57eV. We measured the inhibition zones for *E. coli* (40 mm) and *S. aureus* (40 mm) to evaluate the efficacy of  $\text{Fe}_2\text{O}_3$  NPs as an antibacterial agent. The results of this study demonstrate the ability of  $\text{Fe}_2\text{O}_3$  NPs to protect humans from diseases caused by these microbes.

#### Acknowledgement

The authors gratefully acknowledge the technical support provided by the University of Monastir, Monastir, Tunisia,

#### Conflict of Interest

The authors declare that they have no conflict of interest.

#### References

- [1] N. Ansari, A. Tripathi, S. Ameen, M. S. Akhtar, F. Jabeen, A. Rahman Khan, et al., "Green Synthesis of Nanomaterials: Properties and Their Potential Applications," *Sci Adv Mater*, vol. 16, no. 8, pp. 837–854, 2024.
- [2] S. I. Wanakai, P. G. Kareru, D. S. Makhanu, E. S. Madivoli, E. G. Maina, and A. O. Nyabola, "Catalytic degradation of methylene blue by iron nanoparticles synthesized using *Galinsoga parviflora*, *Conyza bonariensis* and *Bidens pilosa* leaf extracts," *SN Appl Sci*, vol. 1, pp. 1–10, 2019.

- [3] A. Badawi, E. M. Ahmed, N. Y. Mostafa, F. Abdel-Wahab, and S. E. Alomairy, "Enhancement of the optical and mechanical properties of chitosan using Fe<sub>2</sub>O<sub>3</sub> nanoparticles," *Journal of Materials Science: Materials in Electronics*, vol. 28, pp. 10877–10884, 2017.
- [4] B. Rezaei, P. Yari, S. M. Sanders, H. Wang, V. K. Chugh, S. Liang, et al., "Magnetic nanoparticles: a review on synthesis, characterization, functionalization, and biomedical applications," *Small*, vol. 20, no. 5, p. 2304848, 2024.
- [5] P. Maneesard, V. Somsongkul, P. Chirawatkul, C. Saiyasombat, R. Vannier, and C. Kongmark, "Flexible Ni-Based Bimetallic Spinel Oxide (NiM<sub>2</sub>O<sub>4</sub>, M= Mn, Fe, Co) Electrodes for Supercapacitor Applications," *physica status solidi (a)*, vol. 221, no. 23, p. 2400003, 2024.
- [6] S. Chauhan, D. N. Kumar, and L. S. B. Upadhyay, "Facile synthesis of iron oxide nanoparticles using Lawsonia inermis extract and its application in decolorization of dye," *Bionanoscience*, vol. 9, pp. 789–798, 2019.
- [7] M. A. Abid and D. A. Kadhim, "Novel comparison of iron oxide nanoparticle preparation by mixing iron chloride with henna leaf extract with and without applied pulsed laser ablation for methylene blue degradation," *J Environ Chem Eng*, vol. 8, no. 5, p. 104138, 2020.
- [8] S. Lefebure, E. Dubois, V. Cabuil, S. Neveu, and R. Massart, "Monodisperse magnetic nanoparticles: preparation and dispersion in water and oils," *J Mater Res*, vol. 13, no. 10, pp. 2975–2981, 1998.
- [9] Z. J. Zhang, X. Y. Chen, B. N. Wang, and C. W. Shi, "Hydrothermal synthesis and self-assembly of magnetite (Fe<sub>3</sub>O<sub>4</sub>) nanoparticles with the magnetic and electrochemical properties," *J Cryst Growth*, vol. 310, no. 24, pp. 5453–5457, 2008.
- [10] F. J. Kadhim, D. R. M. Ali, A. H. Mohammed, and D. A. Kadhim, "Iron Oxide Nanoparticles were Preparation from Mixing Chitosan Extract with Wasted Iron Extract (Rust) for Photocatalytic Activity," *Journal of Optoelectronics Laser*, vol. 41, no. 3, pp. 183–194, 2022.
- [11] K. G. Gareev, "Diversity of iron oxides: mechanisms of formation, physical properties and applications," *Magnetochemistry*, vol. 9, no. 5, p. 119, 2023.
- [12] N. Fazelian, M. Yousefzadi, and A. Movafeghi, "Toxicity of iron-based nanoparticles to Nannochloropsis oculata: effects of Fe<sub>2</sub>O<sub>3</sub>-NPs on oxidative stress and fatty acid composition," *Marine Biology Research*, vol. 19, no. 2–3, pp. 207–217, 2023.
- [13] S. F. Abbas, A. J. Hadier, S. Al-Musawi, and B. A. Taha, "Synthesis of high-performance antibacterial magnesium oxide nanostructures through laser ablation," *Journal of Applied Sciences and Nanotechnology*, vol. 4, no. 1, pp. 53–65, 2024.
- [14] S. A. Umoren, M. M. Solomon, A. Nzila, and I. B. Obot, "Preparation of silver/chitosan nanofluids using selected plant extracts: Characterization and antimicrobial studies against gram-positive and gram-negative bacteria," *Materials*, vol. 13, no. 7, p. 1629, 2020.
- [15] J. Singh, A. Mehta, M. Rawat, and S. Basu, "Green synthesis of silver nanoparticles using sun dried tulsi leaves and its catalytic application for 4-Nitrophenol reduction," *J Environ Chem Eng*, vol. 6, no. 1, pp. 1468–1474, 2018.
- [16] N. Beheshtkhoo, M. A. J. Kouhbanani, A. Savardashtaki, A. M. Amani, and S. Taghizadeh, "Green synthesis of iron oxide nanoparticles by aqueous leaf extract of Daphne mezereum as a novel dye removing material," *Applied Physics A*, vol. 124, pp. 1–7, 2018.
- [17] S. Nakamura, M. Sato, Y. Sato, N. Ando, T. Takayama, M. Fujita, et al., "Synthesis and application of silver nanoparticles (Ag NPs) for the prevention of infection in healthcare workers," *Int J Mol Sci*, vol. 20, no. 15, p. 3620, 2019.
- [18] M. A. Abid, L. A. Latif, D. A. Kadhim, and W. J. Aziz, "Antimicrobial activity by diffusion method using iron oxide nanoparticles prepared from (Rose plant) extract with rust iron," in *Journal of physics: conference series*, IOP Publishing, 2021, p. 032068.
- [19] M. A. Abid, D. A. Kadhim, and W. J. Aziz, "Iron oxide nanoparticle synthesis using trigonella and tomato extracts and their antibacterial activity," *Materials Technology*, vol. 37, no. 8, pp. 547–554, 2022.
- [20] W. S. Abbas, Z. W. Atwan, Z. R. Abdulhussein, and M. A. Mahdi, "Preparation of silver nanoparticles as antibacterial agents through DNA damage," *Materials Technology*, vol. 34, no. 14, pp. 867–879, 2019.
- [21] R. C. Pawar, S. Kang, J. H. Park, J. Kim, S. Ahn, and C. S. Lee, "Evaluation of a multi-dimensional hybrid photocatalyst for enrichment of H<sub>2</sub> evolution and elimination of dye/non-dye pollutants," *Catal Sci Technol*, vol. 7, no. 12, pp. 2579–2590, 2017.
- [22] Y. C. Zhang, Z. N. Du, K. W. Li, M. Zhang, and D. D. Dionysiou, "High-performance visible-light-driven

- SnS<sub>2</sub>/SnO<sub>2</sub> nanocomposite photocatalyst prepared via in situ hydrothermal oxidation of SnS<sub>2</sub> nanoparticles,” *ACS Appl Mater Interfaces*, vol. 3, no. 5, pp. 1528–1537, 2011.
- [23] N. Benzerroug, D. Makhlouf, and M. Choubani, “Effects of pressure, temperature, and electric field on linear and nonlinear optical properties of In<sub>x</sub>Ga<sub>1-x</sub>As/GaAs strained quantum dots under indium segregation and In/Ga intermixing phenomena,” *Physica B Condens Matter*, vol. 658, p. 414819, 2023.
- [24] F. J. Kadhim, M. H. Bedoui, and A. J. Haider, “Bio-nanocomposites of CS-CuO-AgO from wild shrimp extract via PLA-H method for against *S. aureus* and *E. coli* bacteria,” *Opt Quantum Electron*, vol. 56, no. 7, p. 1185, 2024.
- [25] S. N. Ismail, F. J. Kadhim, and B. A. Yousif, “Iron oxide nanoparticles synthesized from mixing iron (iii) nitrate salt (Fe<sub>2</sub>NO<sub>3</sub>) with (curcumin) herbs extract for antibacterial activity,” *J Surv Fish Sci*, vol. 10, no. 3S, pp. 1455–1464, 2023.
- [26] S. F. Abbas, A. J. Haider, S. Al-Musawi, and M. K. Selman, “Antibacterial effect of copper oxide nanoparticles prepared by laser production in water against staphylococcus aureus and Escherichia Coli,” *Plasmonics*, vol. 19, no. 5, pp. 2401–2411, 2024.
- [27] H. A. Khamees and M. A. Abid, “Effects of Different Biosynthesis Methods on the Structural and Optical Properties of Iron Oxide Nanoparticles and Photocatalytic Application,” *Journal of Nanostructures*, vol. 12, no. 4, pp. 999–1012, 2022.
- [28] D. Fiorani, A. M. Testa, F. Lucari, F. D’orazio, and H. Romero, “Magnetic properties of maghemite nanoparticle systems: surface anisotropy and interparticle interaction effects,” *Physica B Condens Matter*, vol. 320, no. 1–4, pp. 122–126, 2002.
- [29] Z. Jing and S. Wu, “Synthesis and characterization of monodisperse hematite nanoparticles modified by surfactants via hydrothermal approach,” *Mater Lett*, vol. 58, no. 27–28, pp. 3637–3640, 2004.
- [30] G. F. Goya, T. S. Berquo, F. C. Fonseca, and M. P. Morales, “Static and dynamic magnetic properties of spherical magnetite nanoparticles,” *J Appl Phys*, vol. 94, no. 5, pp. 3520–3528, 2003.
- [31] M. Al-Salih, S. Samsudin, and S. S. Arshad, “Synthesis and characterizations iron oxide carbon nanotubes nanocomposite by laser ablation for anti-microbial applications,” *Journal of Genetic Engineering and Biotechnology*, vol. 19, no. 1, p. 76, 2021.
- [32] R. Mehdizadeh, L. A. Saghatforoush, and S. Sanati, “Solvothermal synthesis and characterization of  $\alpha$ -Fe<sub>2</sub>O<sub>3</sub> nanodiscs and Mn<sub>3</sub>O<sub>4</sub> nanoparticles with 1, 10-phenanthroline,” *Superlattices Microstruct*, vol. 52, no. 1, pp. 92–98, 2012.
- [33] R. Gumathannavar, A. Thormothe, P. Bhutada, M. M. Shirolkar, A. Kulkarni, and S. Koratkar, “Chitosan chelated Fe<sup>3+</sup> nanocomposite for enhanced biomedical and environmental applications,” *Nanocomposites*, vol. 9, no. 1, pp. 159–170, 2023.